ORIGINAL PAPER

Preparation of microencapsulated ammonium polyphosphate with carbon source- and blowing agent-containing shell and its flame retardance in polypropylene

**Zaihang Zheng · Linhui Qiang · Ting Yang ·
Bingnan Wang · Xuejun Cui · Hongyan Wang**

Abstract In this paper, a novel and facile method was carried out to microencapsulate ammonium polyphosphate (APP) via two-step surface polymerization process, which introduces the carbon source and blowing agent into the microcapsules simultaneously. The chemical composition of microencapsulated APP (MAPP) was confirmed by fourier infrared spectra (FTIR). The surface morphology and thermal behavior of APP and MAPP were investigated by scanning electron microscope (SEM) and thermogravimetric analysis (TGA), respectively. Additionally, transmission electron microscopy (TEM) demonstrates that MAPP particles possess the obvious "core/shell-like" structure. Compared with APP, the water solubility of MAPP greatly decreases that can improve the water resistance of MAPP in polymer materials when exposed to water. Moreover, the flame retardant properties of polypropylene (PP) compositing with MAPP were systematically researched by limiting oxygen index (LOI), vertical burning tests (UL-94) and cone calorimeter. The results show the flame retardant properties of PP composites are enhanced by combining MAPP than that of APP. Besides, the water resistance of PP/MAPP is also enhanced. And the char residue of PP composites after combustion was analyzed by FTIR and X-ray photoelectron spectroscopy (XPS) spectra. Based on these facts, a possible flame retardant mechanism of MAPP in PP composites was proposed.

Z. Zheng · L. Qiang · T. Yang · B. Wang · X. Cui · H. Wang (✉)
College of Chemistry, Jilin University, Changchun 130012,
People's Republic of China
e-mail: wanghongyan505@yeah.net

Introduction

As we know, polypropylene (PP) is one of significant general commodity plastics [1], which has extensive application in many fields such as wire, cables, automobiles, packaging etc. However, its inflammability when exposed to fire restrains its application for PP materials in some fields [2]. Recently, halogen-free intumescent flame retardant (IFR) has attracted a large amount of attention in flame-retarding PP materials [3–8]. Compared with halogen-containing flame retardants, halogen-free intumescent flame retardants have more advantages in actual utilization, such as low smoke release, anti-dripping property and toxic gases generation during combustion. Until now, the most typical and widely researched IFR system is the combination of an acid source, a carbon agent and a gas source. Besides, the most outstanding ternary IFR system is a mixture of ammonium polyphosphate (APP), pentaerythritol (PER) and melamine (MEL) and its main flame retardant mechanism is depicted as follows. On one hand, the dilution effect of inert gases originating from gas source (MEL) that can decrease the oxygen concentration around the atmosphere of fire and take the heat from the combustion zone; on the other hand, the dense and compact char layer structure formed by the esterification reaction between APP and PER can act as a physical barrier, which greatly limits heat and mass transfer between gas and condensed phases [9]. In this condition, the flame retardant

properties of materials can be improved by the combination of the two ways. Bourbigot and co-workers have performed extensive studies on this IFR system in polyolefins and have reviewed recent development of IFR systems in field of flame retardant materials in great details [10–12]. A series of successful and valuable conclusion has been achieved and can effectively instruct the application of flame retardants in polymer materials.

Unfortunately, the APP/PER/MEL system is not durable due to the weak water resistance and thus is easily attacked by water. Thus, when polymer materials are exposed to water or moisture environment, migration and exudation of them may occur, which results in a decrease in the flame retardancy and mechanical properties of polymer composites [13]. Besides, the poor compatibility due to the large surface energy difference between inorganic flame retardants and organic polymer materials also restricts the application of the IFR system. To deal with these shortcomings, microencapsulation technology with water insoluble materials is usually employed to modify the flame retardants. As previous reports, the microencapsulation materials include melamine formaldehyde resin (MF) [14–16], epoxy resin (EP) [17], urea-melamine-formaldehyde resin (UMF resin) [18], poly(vinyl alcohol)-melamine-formaldehyde resin [19] and polyurethane [20]. In these experiments, lots of valuable results were obtained in improving the disadvantages of flame retardants. However, these microencapsulation materials themselves cannot effectively act as flame retardants in IFR system. In our previous work, APP particles had been successfully microencapsulated via surface polymerization process [21] and have been applied in flame-retardaning rigid polyurethane foam with expandable graphite. By this method, the blowing agent (MEL) has been successfully introduced into the microcapsules. However, few experiments are carried out via two-step surface polymerization to microencapsulate APP by the introduction of carbon source- and blowing agent-containing into the microcapsules simultaneously.

In this paper, microencapsulated APP (MAPP) particles were prepared via in situ two-step surface polymerization with 4, 4′-diphenylmethane diisocyanate (MDI), melamine (MEL) and pentaerythritol (PER). The aim of this article is to solve the drawbacks existing in APP and introduce the flame retardants into the surface of APP, which are described as follows. In one hand, the ternary intumescent flame retardant system (APP/PER/MEL) is combined via the microencapsulation process in one compound; in the other hand, the property of APP as flame retardant can be improved by this method, such as compatibility with polymer materials, water resistance and flame retardancy. The chemical composition of MAPP was certified by fourier transform infrared (FTIR). Except that, transmission electron microscopy (TEM) demonstrates that MAPP particles possess the obvious "core/shell-like" structure. Therefore, it can construct and form more simple and environment-friendly intumescent flame retardant complex system via the introduction of carbon source (PER) and blowing agent (MEL) into the microcapsules on the surface of MAPP. Moreover, the thermal properties and flame retardancy of polymer composites have been systematically investigated. Based on the detailed analysis for char residue of PP/MAPP after combustion, the possible flame retardant mechanism was primarily proposed.

Experimental

Materials

PP (melt-flow rate 2.5 g/10 min) was provided by Yangzi Petroleum Chemical Company. Ammonium polyphosphate (APP) (phase II, the degree of polymerization >1500; density, 1.88 g/cm^3) brought from Qingdao Haida Chemical Co., Ltd. was under 80 °C vacuum drying before using. 4, 4′-diphenylmethane diisocyanate (MDI) was obtained from Yantai Wanhua Polyurethanes Co., Ltd. Pentaerythritol (PER) and melamine (MEL) purchased from Aladdin were dried at 80 °C for 24 h. Ethyl acetate obtained from Aldrich was removed water through distillation before using. The water used in this experiment was distilled followed by deionization.

Preparation of microencapsulated APP

Microencapsulated APP was carried out under nitrogen atmosphere in a 1,000 ml four-neck flask equipped with reflux condenser, mechanical stirrer, dropping funnel are heated in the water bath. At first, 50 ml ethyl acetate and 100 g APP were introduced into the flask with a stirring speed of 300 rpm. When the mixture was heated to about 55 °C, MDI solution (10 g MDI dissolved in 50 ml ethyl acetate) and MEL dispersion liquid (4.8 g MEL dispersed in 50 ml ethyl acetate) were dropped into the above flask. The system maintained at 55 °C for 5 h. Then, the mixture was heated to 75 °C, MDI solution (10 g MDI dissolved in 50 ml ethyl acetate) was dropped to the flask within 15 min and reacted for 3 h. After that, PER dispersion liquid (20 g PER dispersed in 50 ml ethyl acetate) was poured into the flask and kept for another 3 h. At last, the mixture was filtered instantly under the condition of vacuum. Besides, the product was washed with ethyl acetate for 2–3 times and with 60 °C deionized water for 2–3 times. Finally, moist production was dried at 70 °C for overnight. Thus, microencapsulated APP powder was obtained. The microencapsulation procedure was shown in Scheme 1.

Preparation of polyurethane (PU) polymer

PU polymer which used to microencapsulate APP was also synthesized. The preparation of PU polymer was the same as
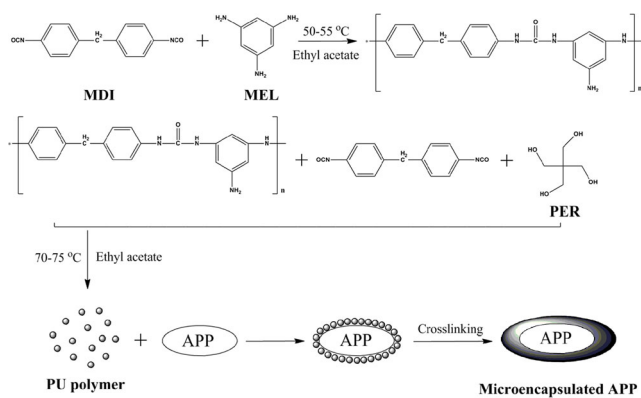
Scheme 1 The microencapsulation process of MAPP

the microencapsulation process of APP. Different from the microencapsulation of APP, PU polymer were synthesized in absence of APP particles.

Simulation details

The simulation was conducted with the Materials Studio v5.0 package (Acclrys) using the condensed-phase optimized molecular potentials for atomistic simulation studies (COMPASS) force field. The molecular structure of PP, APP and PU polymer are shown in Scheme 2. The PP chain and APP chain were constructed with the 100 repeat units and 25 repeat units, respectively. The PU polymer possesses a block structure and there were two chain units in a PU polymer chain. Based on the structure of microcapsules, the chain units were built by $[AB]_{10}$ and $[AC]_{10}$ (where A, B and C represents MDI, MEL and PER), respectively. Besides, the interface models have been structured by stacking the layer models. The APP/PP interface model contains the surface of APP particles and PP polymer chains layer models, while the APP/PU/PP interface model contains three "sandwich-like" layers, such as APP surface layer model on the bottom, PP polymer chains layer model on the top and PU polymer chains layer model in the middle. Thus, the APP surface layer model has been obtained by putting two APP polymer chains in an amorphous cell with the amorphous cell program. After that, the APP amorphous cell was optimized by the steepest decent and conjugate gradient method. To reach an energy-minimized state, the APP amorphous cell was annealed by performing dynamics simulations for 100 ps at each temperature, which increased from 300 to 600 K and then decreased to 300 K with a step of 50 K. After the annealing, 200 ps NPT MD simulation was performed at 453 K with 1 fs time step. Finally, the APP surface layer model was obtained and the density of APP amorphous cell was about 1.9 g/cm^3 which was close to the experimental value. Besides, the layer models of PP and PU polymer chains were structured by using the same method. Then both of them were performed by annealing with MD simulation in the same condition. The density of

PP amorphous cell after annealing and NPT MD was close to the experimental value (about 0.9 g/cm^3) [22].

After three kinds of layer models structured, the APP/PP and APP/PU/PP interface models were easily obtained. Then two kinds of interface models have performed the 500 ps NVT MD simulation at 453 K (process temperature). Trajectories where saved every 2 ps and the final 50 ps configurations were used for analysis of interaction energy and radius distribution function (RDF) of interface models. During the whole simulation process, the temperature and pressure were maintained by Andersen and Berendsen method, respectively.

Preparation of flame-retarding PP composites

PP and flame retardants were melt-mixed in a twin-roller mill (manufactured by Wuhan Ruiming Plastic Machinery Factory, SJSZ-10) at a temperature about 180–190 °C for 15 min. The roller speed was 30 rpm. After mixing, the samples were hot-pressed at about 190 °C under 10 MPa for 10 min into sheets of suitable size for measurements. The detailed formulations are given in Table 1.

Materials characterization

Fourier transform infrared spectra (FTIR)

The infrared spectra of the samples were recorded with a FTIR SHIMADZU spectrometer at a resolution of 2 cm^{-1}. FTIR spectra of the samples were obtained between 4,000 and 400 cm^{-1} on a KBr powder with an FTIR spectrometer.

Scanning electron microscope (SEM)

The morphology of APP and MAPP after gold-sputtered were investigated by SHIMADZU SSX-550 scanning electron microscope (SEM). And PP composites were fractured in liquid nitrogen. The specimens were sputter-coated with a conductive layer. The accelerated voltage was 20 kV.

Transmission electron microscopy (TEM)

The samples were dispersed ethanol and sonicated for 15 min before measurements. The experiments were performed on a TEM H-800 of HITACHI Company with an accelerating voltage of 200 kV.

Thermogravimetric analysis (TGA)

All of samples were dried overnight before measurement. The TGA curves were recorded on a Pyris Diamond TG/DTA (Perkin Elmer, USA) under 50 ml/min nitrogen flow ratio from 50 to 850 °C at a heating rate of 10 °C/min. The weight of samples was 5–10 mg.

Scheme 2 The molecular structure of PP, APP and PU polymer (Carbon: *gray*; Hydrogen: *white*; Oxygen: *red*; Nitrogen: *blue*; Phosphorus: *pink*)
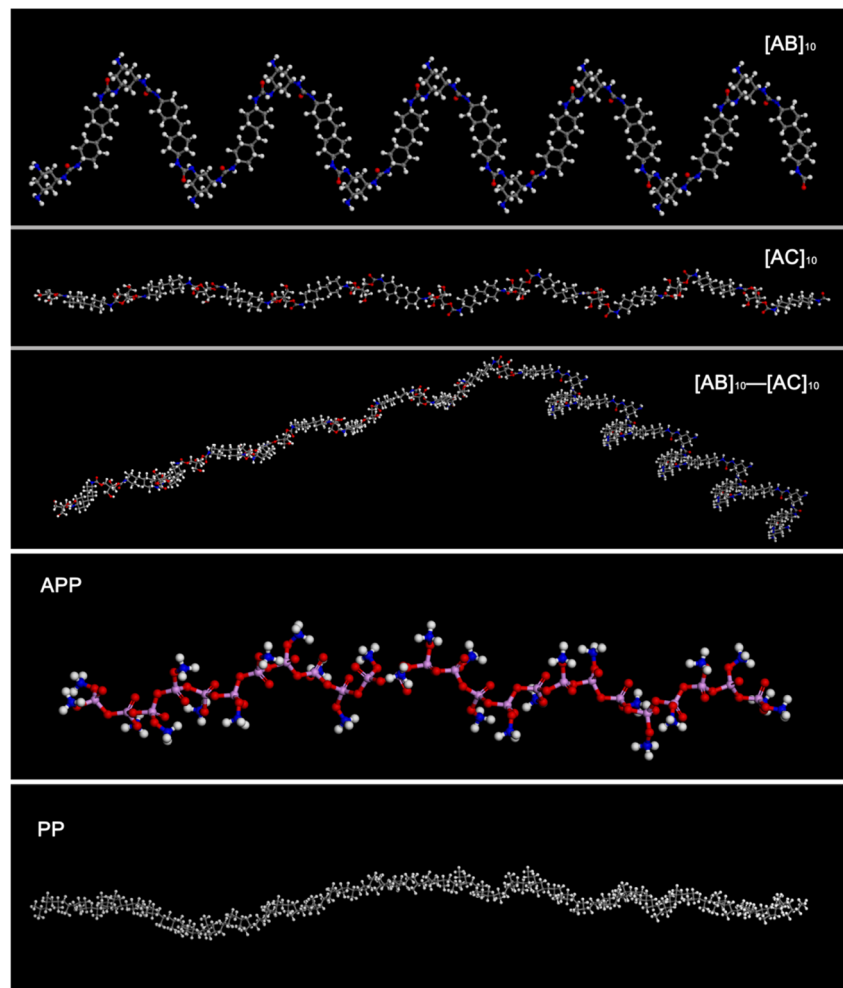
X-ray photoelectron spectroscopy (XPS) spectra

The XPS spectra were recorded with a VG ESCALAB MK II spectrometer using Al ka excitation radiation (hν = 1253.6 eV).

Water solubility tests

Weighed APP or MAPP (about 5 g) was put into 250 ml flask with 100 ml deionized water, and kept stirring at a constant temperature of 25, 50 and 75 °C for 2 h, respectively. After that, filtered the mixture rapidly, and toke 10 ml liquid filters into a glass watch (weight W_0), dried in the oven at the temperature of 70–90 °C until the water was absolutely removed. The weight of glass watch was labeled as W_1. The water solubility of APP was calculated as followed.

$$\text{Water solubility of APP}(g/100 \text{ ml } H_2O) = (W_1-W_0)/10 \times 100.$$

Particle size distribution measurement

The mean particle size and distribution of APP and MAPP were measured by Laser particle sizing instrument (LS320) of Beckman Coulter, Inc, USA. Before the measurement, the samples were dispersed in ethanol and sonicated for 15 min.

Table 1 The formulations of PP composites

Sample code	PP (wt%)	APP (wt%)	MAPP (wt%)	LOI (%)		UL-94	
				Untreated	Treated	Untreated	Treated
PP	100	0	0	17.0	17.0	No rating	No rating
PP/APP	70	30	0	20.0	17.5	No rating	No rating
PP/MAPP	70	0	30	25.0	24.0	V-1	V-1

Water contact angle test

Water contact angle tests were measured with a JC2000C2 contact angle goniometer (Shanghai Zhongchen Powereach Company, China) by the sessile drop method with a microsyringe at 25 °C. More than 10 contact angles were averaged to get a reliable value for each sample.

Limiting oxygen index (LOI)

The LOI tests were carried out by using an XZT-100A oxygen index test instrument (Chengde Jiande test instrument Co., Ltd., China) based on the standard LOI test, ASTM D 2863-97. The dimensions of specimens were $127 \times 10 \times 10$ mm^3.

Vertical burning tests (UL-94)

UL-94 tests were performed with plastic samples of dimensions $130 \times 13 \times 3$ mm^3, suspended vertically above a cotton patch. The classifications are defined according to the American National Standard UL-94. Five specimens were taken to estimate the precision of the reported data.

Cone calorimeter

The cone calorimeter (Stanton Redcroft, UK) tests were performed according to ISO 5660 standard procedures. Each specimen of dimensions $100 \times 100 \times 3$ mm^3 was put on a horizontal aluminium tray and exposed horizontally to an incident and external heat flux of 35 kW m^{-2}. Flame-out was defined as the extinguishment of the visible yellow flame. The value for amount of residue was taken at flame-out, which was characterized as the flaming burning before the residues were consumed in the subsequent afterglow. In additional experiments fire residues were removed from the cone calorimeter at flame-out and quenched with liquid nitrogen in order to avoid thermooxidation of the subsequent afterglow and thus to observe the residue structures formed during combustion. Time to ignition (TTI), total heat release (THR), peak of heat released rate (p-HRR) and amount of residue after combustion will be obtained and discussed. Results correspond to mean values obtained from two or three experiments. The experimental error for all the mentioned parameters is ±10 %.

Results and discussion

FTIR spectra of MAPP

FTIR spectra of APP, PU polymer and MAPP are shown in Fig. 1. The typical absorption peaks of APP contain 3200 (N-H), 1256 (P = O), 1075 (P-O symmetric vibration), 1020
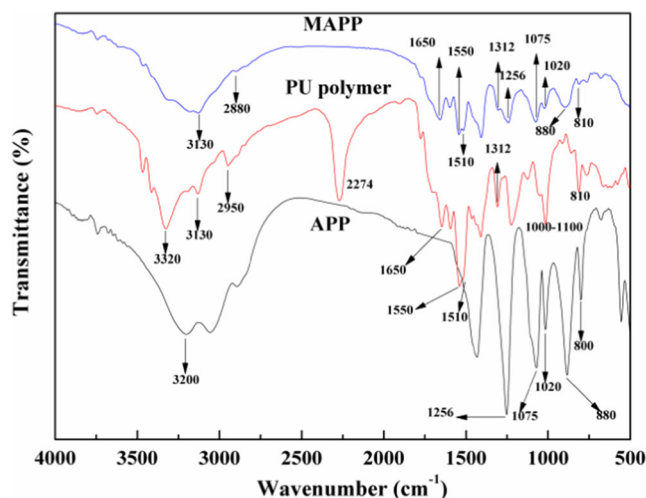

Fig. 1 FTIR spectra of MAPP

(symmetric vibration of PO$_2$ and PO$_3$), 880 (P-O asymmetric vibration), 800 (P-O-P) cm^{-1} [23, 24]. FTIR spectra of PU polymer mainly includes 1,000–1,100 cm^{-1} and 810 cm^{-1} (the absorption peaks of benzene from MDI), 1,550, 1,510 and 1,312 cm^{-1} (from MEL) [25–28], 2,274 cm^{-1} (-NCO groups from MDI), 3,130 cm^{-1} (-NH$_2$ groups on MEL), 2,950 and 3,320 cm^{-1} (-CH$_2$- and -OH groups on PER). Moreover, the characteristic absorption peak of 1,650 cm^{-1} is attributed to -C(=O)- groups (-NH-C(=O)-NH- or -NH-C(=O)-O-) on the PU molecules. For MAPP, the main absorption peaks are as follows: 3,130, 2,880, 1,650, 1,550, 1,510, 1,400, 1,312, 1,256, 1,075, 1,020, 880 and 800 cm^{-1}. The peaks at 1,550, 1,510, 1,312 cm^{-1} are from MEL on PU polymer. Besides, the characteristic peak at 1,650 cm^{-1} is generated from the -C = O groups on PU molecules, which is well consistent with the FTIR spectra of PU polymer. Moreover, due to the complete reaction among MDI, MEL and PER on the surface of APP, the absorption peak of 2,274 cm^{-1} (-NCO) disappears on the FTIR spectra of MAPP. Therefore, FTIR spectra of MAPP demonstrates not only the characteristic absorption peak of APP, but also the absorption peak of PU polymer, illustrating the PU microcapsules exist on the surface of MAPP.

Surface morphology of MAPP

The surface morphology of APP and MAPP was observed by SEM, as shown in Fig. 2. It can be obviously observed that the severe aggregation phenomenon appears among APP particles, which can lead to the poor dispersion and bad compatibility of APP in polymer materials. After microencapsulation, the agglomeration effect is greatly weakened and the cluster diameter of MAPP particles is much smaller than that of native APP, as presented in Fig. 2b. Besides, pure APP particles present a smooth and club-shaped surface morphology with sharp ends [29]. After modification, the surface of MAPP
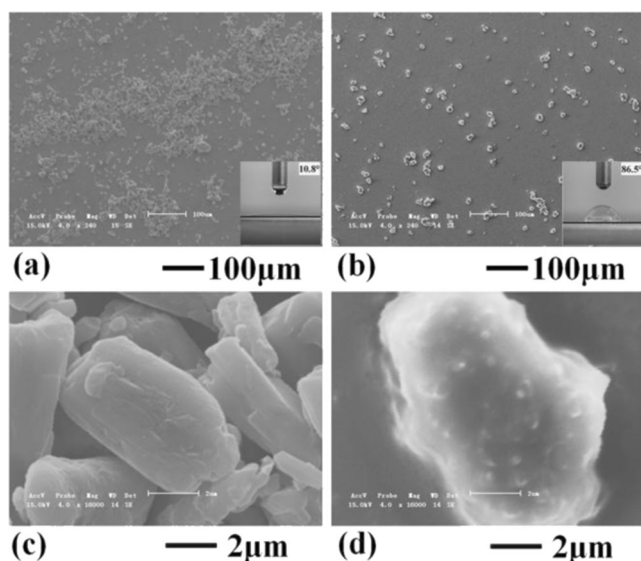
Fig. 2 SEM and contact angle photos of APP and MAPP
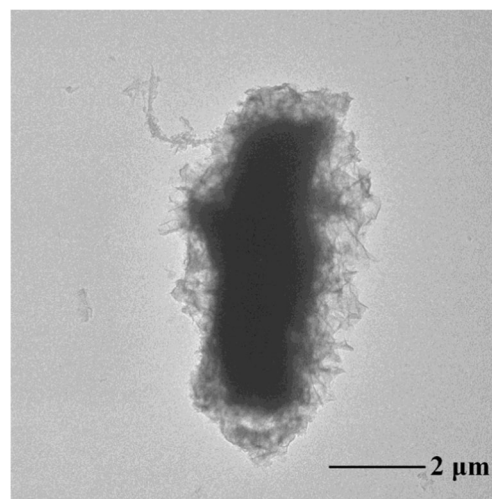

Fig. 3 TEM photos of MAPP

becomes much rougher than that of APP. Compared with pure APP, the sharp ends disappear after microencapsulation, as shown in Fig. 2d. Therefore, we can conclude that bare APP particles are well coated by the PU microcapsules.

Water contact angle of MAPP

To investigate the surface property of APP and MAPP, the water contact angle tests were carried out. As we know, water contact angle tests could evaluate the surface hydrophobicity of solid powder. As exhibited in Fig. 2, due to $-NH_4$ groups on molecular chain of APP, the water contact angle of APP is only $10.8°$. This indicates that pure APP is hydrophibic with high surface energy and easily attacked by the influence of water or moisture. Traditionally, it is considered that with the polarity of powder or membrane materials decreasing, its surface energy accordingly decreases and its water contact angle accordingly increases to some extent. Thus, due to the formation of the weak polar PU microcapsules (prepared in this article) on the surface of APP, the surface energy of MAPP is greatly decreased. In this condition, the water contact angle of MAPP reaches $86.5°$. When MAPP particles are incorporated into polymer matrix, the compatibility between MAPP and polymer materials will be improved, which is generated from the contractible polar gap between flame retardants and polymer matrix. In brief, this phenomenon can be illustrated by the formation of PU microcapsules on surface of APP.

Transmission electron microscopy of MAPP

The morphology of MAPP was also characterized by transmission electron microscopy (TEM), as presented in Fig. 3. As we know, TEM tests are one of best and intuitive methods

to evaluate the morphology of particles. As shown in Fig. 3, an obvious light shadow (about 0.5–1.5 μm) is appeared around the club-shaped MAPP particles. In another word, after microencapsulation, MAPP particles possess the obvious "core/shell-like" structure which the core is APP particles, while the shell is PU microcapsules. Along with the results of FTIR spectra and SEM, this fact can further illustrate the formation of PU microcapsules on the surface of APP. And this "core/shell-like" PU microcapsules formed by the reaction of MDI, MEL and PER will play a significant role in weakening the aggregation of APP particles, enhancing the water resistance of APP and improving the dispersion and compatibility of APP particles in polymer matrix via decreasing the surface energy.

Thermal behavior of MAPP

The thermal behavior of APP and MAPP were investigated by TGA, as shown in Fig. 4. Besides, the differential thermal gravity (DTG) of TGA curves was also investigated in Fig. 4. It can be observed that the thermal degradation curve of APP is mainly composed of two steps. In first step, APP presents an obvious decomposition at 300–530 °C with about 20 wt.% weight loss, which is attributed to the release of the volatile products (NH_3 and H_2O) and the formation of a highly crosslinked polyphosphoric acids (PPA) [30–32]. With the temperature increasing, the further decomposition of PPA leads to the formation of P_2O_5 and P_4O_{10} in second step, which leaves 14 wt.% residual weight. However, the thermal decomposition process of MAPP is mainly composed of three steps in DTG curve. It can be observed that the initial degradation temperature of MAPP is much lower than that of APP, which is mainly due to the low thermal stability of microcapsules on the surface of MAPP. The thermal decomposition of microcapsules will produce the inert gases (NH_3 and H_2O, from MEL), which can enhance the gas flame-retarding
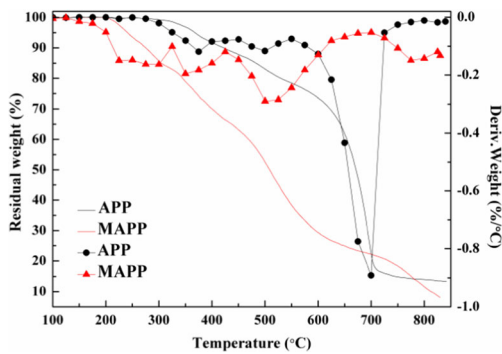
Fig. 4 Thermal behavior of APP and MAPP

function of APP particles by way of diluting the oxygen concentration around the zone of fire. In second stage, APP starts to decompose to form inert gases and PPA at 300 °C, which is well consistent with that of APP. Besides, the temperature at the maximum weight loss of MAPP is much lower than that of APP. Surprisingly, the maximum weight loss rate of MAPP is much lower than that of APP. These facts may be ascribed to that the thermal stability of char residue via the prompt chemical reaction between PPA and PER (on microcapsules) improves the char-forming rate and possesses higher thermal stability than PPA generating from APP particles. And the char residue with the crosslinking structure (P-O-C) will slow down the thermal degradation rate of PP materials. Thus, it will take effect in the condensed phase for flame-retarding polymer materials. However, when the temperature of MAPP is higher than 800 °C, the residual weight is slightly lower than that of APP. It is because of the initial degradation of microcapsules (MEL section) to form the inert gases.

Particle size and its distribution of MAPP

As shown in Fig. 5, the particle size and its distribution of APP and MAPP were analyzed by laser particle size instrument. It is obviously observed that the number-average diameter of MAPP (4.9 μm) is much smaller than that of APP (10.7 μm). This can be attributed to the fact that compared with pure APP,
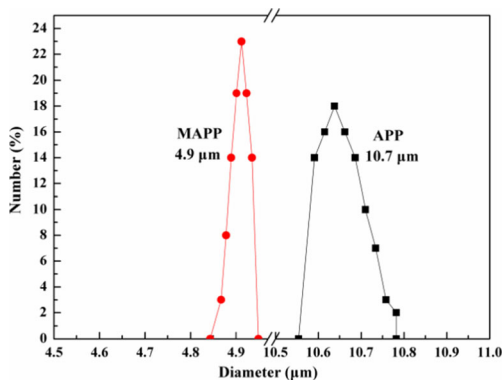

Fig. 5 Particle size and its distribution of APP and MAPP

the particle agglomeration size of MAPP diminishes after coating with PU microcapsules. Moreover, the particle size distribution of MAPP is narrower than that of native APP. For these facts, it is expected that MAPP will have better dispersion in PP matrix than APP when they are blended with PP matrix, results in a better flame retardant properties.

Water solubility of MAPP

The water solubility of APP and MAPP at different temperature was also investigated and the detailed data is shown in Table 2. As we know, APP is easily attacked by moisture or water, especially at high temperature [33]. The water solubility of APP at 25, 50 and 75 °C is 0.50, 1.60 and 2.90 g/100 ml H$_2$O, respectively. This shortcoming can lead to the exudation of flame retardant from polymer matrix when exposed to a damp environment, which will deteriorate the flame retardant property of materials. After microencapsulation, the water solubility of MAPP is sharply reduced. At 75 °C, the water solubility of MAPP decreases by about 73 %. These facts can be illustrated that the PU microcapsules on the surface of APP are hydrophobic, leading to a decrease in the water solubility and an increase in the durability of APP.

Interface morphology of PP/MAPP

Moreover, in order to confirm and investigate the dispersion of flame retardants in PP matrix, the fracture section morphology of PP composites were carried out by SEM images, as shown in Fig. 6. It can be observed that there are a lot of cavities and cracks on the surface of fracture section for PP/APP composites. Besides, it can be seen that obvious gaps and interfaces between PP matrix and APP particles, as shown in Fig. 6a, b and c. This phenomenon may be attributed to the large different polarity diversity between inorganic flame retardant particles and PP matrix, which makes them thermodynamically immiscible. In this condition, it causes a loose and weak interfacial adhesion between polymer materials and fillers, which is labeled by arrows in Fig. 6c. It is well consistent with the facts of WCA tests. However, as presented in Fig. 6d, e and f, it can be found that MAPP has well dispersion in the PP matrix compared with that of APP particles. Compared with PP/APP, the defects existing in the interface between fillers and PP matrix for PP/MAPP system

Table 2 Water solubility of APP and MAPP

| Sample code	25 °C (g/100 ml H$_2$O)	50 °C (g/100 ml H$_2$O)	75 °C (g/100 ml H$_2$O)
APP	0.50	1.60	2.90
MAPP	0.06	0.39	0.77

Fig. 6 Interface morphology of PP/APP and PP/MAPP, **a** PP/APP (20 μm), **b** PP/APP (10 μm), **c** PP/APP (5 μm); **e** PP/MAPP (20 μm), **f** PP/MAPP (10 μm), **g** PP/MAPP (5 μm)
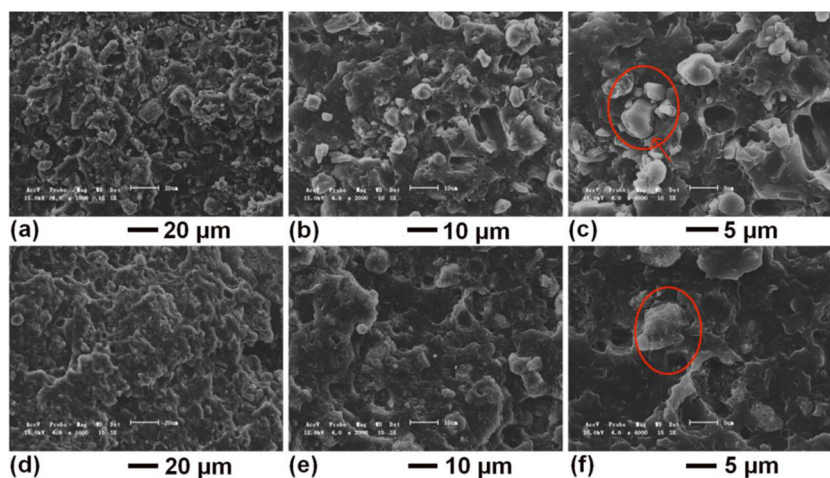
decrease to some extent. In addition, the compatibility between flame retardant particles and PP matrix are enhanced from the reduction in the gaps for interfaces. As it is expected, the PU microcapsules on the surface of MAPP after co-microencapsulation play a significant role in connection and adhesion between inorganic flame retardants and polymer matrix. Therefore, when MAPP is incorporated into PP composites, it can greatly improve the dispersion and compatibility of MAPP and PP matrix, which can further enhance the flame retardant properties of PP composites to some content. Except that, the binding energy analysis of PP composites was systematically investigated by MD simulation as follows. This method can deeply illustrate the reason of the enhanced interface compatibility for PP/MAPP.

Binding energy analysis by MD simulation

After the MD simulation, the equilibrium interface models have been obtained in Fig. 7. The interaction energy (E_i) can reflect the interfacial compatibility and stability to some extent. The E_i value between two components (alternative two
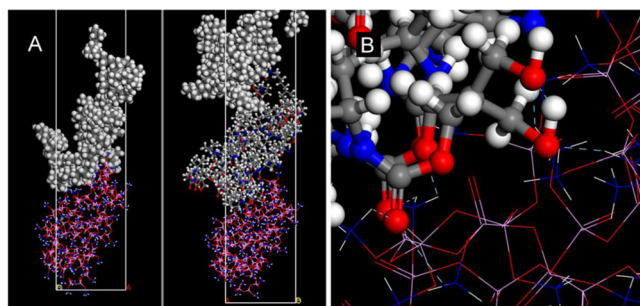
Fig. 7 The equilibrium interface models, **a** Molecular layer models of PP/APP (*left*) and PP/MAPP (*right*), **b** The possible hydrogen bonding between APP and PU microcapsules in PP/MAPP (PU microcapsules in *ball-stick module*, while APP in *line module*). Carbon: *gray*; Hydrogen: *white*; Oxygen: *red*; Nitrogen: *blue*; Phosphorus: *pink*

substances in PP, APP and PU polymer) can be calculated by the following equation (Eqs. 1–3), respectively.

$$E_{i(PP-APP)} = E_{T(PP-APP)} - E_{PP} - E_{APP} \qquad (1)$$

$$E_{i(PP-PU)} = E_{T(PP-PU)} - E_{PP} - E_{PU} \qquad (2)$$

$$E_{i(APP-PU)} = E_{T(APP-PU)} - E_{APP} - E_{PU} \qquad (3)$$

Where E_T represents for the energy of two components after MD simulation and E_{PP}, E_{APP}, E_{PU} represent the energy of PP, APP and PU polymer, respectively.

Table 3 presented the interaction energy of different interfaces which belong to PP/APP and PP/PU/APP system. It can be found that the E_i value of PP/PU interface was larger than that of the APP/PP interface. The possible reasons might be the strong interaction between PP molecular chain and the non-polar units on PU polymer chain. Therefore, the PP/PU interface has much better interfacial compatibility and stability than the PP/APP interface. And the E_i value of PU/APP interface is −31,576 kcal/mol, which is far greater than that of other interfaces. It might be caused by forming the hydrogen bond between PU and APP. For PU and APP molecular chains, there are many high activity acceptors and donors which could form hydrogen bonds easily. Although the hydrogen bonding action could not be obtained through COMPASS force-field directly, we could study the possible hydrogen bonds via investigating the distance and angle between acceptors and donors on the MD simulation profiles. The dot line shows the possible hydrogen bond on a part of the PU/APP interface (see Fig. 7). Akten et al. have reported another

Table 3 The detailed data of interaction energy

Sample	E_T kcal/mol	E_{APP} kcal/mol	E_{CAP} kcal/mol	E_{PP} kcal/mol	E_i kcal/mol
APP/PP	255252	256009	–	1505	−2263
PP/PU	2111	–	2435	3750	−4074
PU/APP	374430	403571	2435	–	−31576

method to estimate the homogeneity of composite by using radial distribution functions (RDF) [34]. The RDF represents the probability density of A and B at a distance of r with respect to the bulk phase in a completely random distribution. For an immiscible system, the RDF curve of each component exhibits a stronger first maximum than that of the composite [22]. Therefore, the compatibility of PP/APP and PP/PU/APP system could be further investigated by calculating the RDF among the PP, PU and APP. Figure 8 shows the RDF curves of PP-PP and APP-APP were far higher than that of PP-APP, which indicates PP/APP system is immiscible. The PP/PU/ APP system shows a different trend in Fig. 8. The RDF curve of PP-PU indicates that the closest distance between PP and PU molecular is located in range of 3–5 Å, which is a type distance of a strong vdW interaction between two molecules [35]. Simultaneously, the RDF curves of PP-PU and PP-PP exhibit the same trend. It means that the compatibility between PP and PU was much better than the PP/APP system. Based on Fig. 8, the closest distance between PU and APP molecular was about 2.5 Å which might be formed by hydrogen bond interaction. The same results have been obtained by interaction energy and MD simulation profile analysis. This strong interaction between PU and APP makes their interface stability and molding easily. As we expected, these facts was well consistent with that of SEM photos (Fig. 6) that demonstrates that the compatibility between PP matrix and MAPP particles is enhanced via the microencapsulation process.
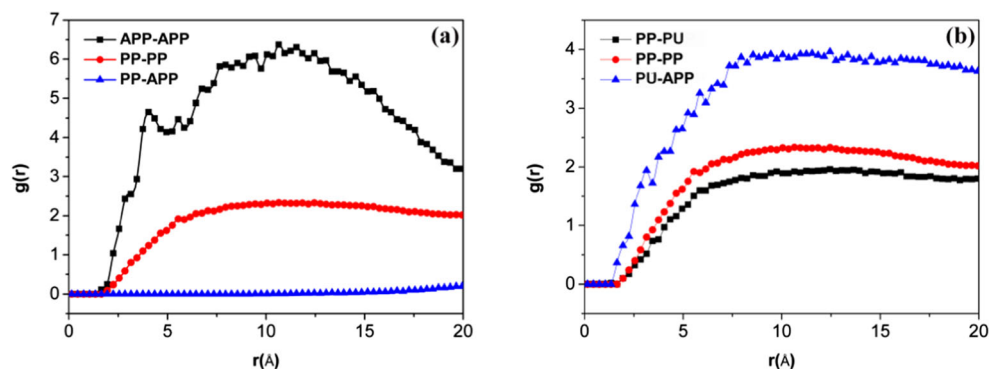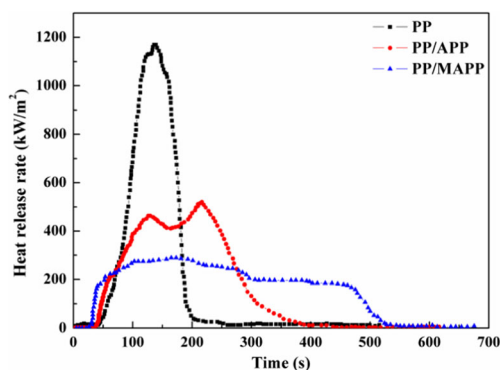
Flame retardant properties of PP composites

As we know, limiting oxygen index (LOI) and vertical burning (UL-94) tests have been widely employed to evaluate the flame retardant properties of materials. The results are recorded in Table 1. As shown in Table 1, the LOI value of pure PP is 17.0. It indicates that PP is easily inflammable material. Besides, neat PP cannot pass the UL-94 tests because of severe melt dripping phenomenon. When PP is composited with APP particles, the LOI value of PP/APP reaches 20.0. Due to lack of char agent, pure APP particles are not very effective in flame-retarding PP materials when used alone. In this condition, PP/APP still cannot achieve the ratings in the UL-94 tests. However, the flame retardant properties of PP composites are greatly improved via combining with MAPP. In detail, PP/MAPP can achieve the LOI value of 25 % and obtain a V-1 rating in UL-94 tests. This is mainly attributed to that charring agent (PER) and gas source (MEL) are introduced to the surface of APP particles after microencapsulation. The possible reason for this phenomenon is proposed as follows. On one hand, the char residues formed by the chemical reaction of -OH groups (from PER) and -POOH (from APP) during combustion can restrain the heat and mass transfer between gas phase and solid condensed phase to some extent; on the other hand, the inert gases (NH_3 and H_2O) from the thermal degradation of APP and MEL can dilute the oxygen concentration around fire source and promote the fast generation of intumescent char layer. Due to these facts, flame retardant properties of PP/MAPP composite are improved. The detailed flame retardant mechanism will be discussed and confirmed in the subsequent part.

Besides, the flame retardant properties of PP composites after treating in 60 °C water for 24 h were also measured. As shown in Table 1, the flame retardancy of PP/APP greatly decreases after water treatment. This is mainly because virgin APP particles are easily attacked by water, especially hot water. After treatment, APP particles exude and migrate from PP matrix to the surface of PP composites, which leads to the

Fig. 8 The RDF curves of PP composites, **a** PP/APP, **b** g(r) of the intermolecular PP-MAPP pairs of different composites

Fig. 9 The HRR curves of PP composites

decrease in flame retardancy. Surprisingly, the flame retardant property of PP/MAPP is nearly not affected by hot water. After microencapsulation, the water solubility of MAPP particles greatly decreases, which leads to the maintenance of LOI value for PP/MAPP after water treatment. Moreover, PP/MAPP after water treatment still maintains V-1 level in UL-94 tests. These facts state that the flame retardant durability of PP composites by combining with MAPP is enhanced when exposed to hot water.

Cone calorimeter study

As we know, cone calorimeter tests are an effective approach to evaluate the combustion behavior of flame-retarding polymeric materials. It is useful for the small scale assessment of several reactions of fire parameters, and this method is widely employed for the development of new materials [36]. The heat release rate (HRR) curves of PP composites are shown in Fig. 9. Besides, the values of time to ignition (TTI), peak heat release rate (p-HRR), total heat release (THR) and residual mass are recorded in Table 4. It can be observed that PP without flame retardant burns very fast after ignition with a p-HRR value of 1174.7 kW/m^2. The p-HRR value of PP/APP decreases to 526.5 kW/m^2, which demonstrates that APP can take effect in flame-retarding PP to some content. However, p-HRR value of PP/MAPP is much lower than that of PP/APP. Except that, it can be observed that the HRR curve of PP/APP shows two peaks in Fig. 9. The first HHR peak for PP

composites is assigned to the gradual formation of the swollen protective char layer by the interaction between flame retardant particles (APP). After the first HRR peak, the second HRR peak appears an increase for PP/APP, in which the increase in HHR value is not restrained and suppressed due to the presence of the ineffective protective char layer on the surface of PP composites during combustion. Compared with PP/APP, the HRR curve of PP/MAPP nearly presents a plateau with low HRR value which indicates that the efficient protective char layer gradually forms as PP composites are continuously exposed to the fire. In the condition, the "barrier effect" of protective char layer for PP/MAPP during the thermal degradation can leads to the reduction in HHR value [37, 38]. In case of PP/MAPP, the p-HRR value is much lower than that of PP/APP. Besides, the combustion time of PP/MAPP is prolonged than pure PP and PP/APP, as shown in Fig. 9. Obviously, the thermal decomposition rate for PP/MAPP tends to slow down with the time. This phenomenon is originated from the formation of more effective, dense and thermal-stability char layer during combustion. The char layer may be mainly ascribed to the chemical reaction between APP and PER from PU microcapsules to generate the crosslinking bonds, which can promote the formation of high-quality char layer during combustion of PP/MAPP. The char layer can prevent the matrix from contacting with heat and oxygen effectively, resulting in a lower p-HRR value. Conclusion can be made from above results that it can form an efficient intumescent protective char in PP/MAPP and thus results in a decrease of HHR value than PP/APP composites. As presented in Table 4, the THR value of pure PP is 102.2 MJ/m^2. However, PP/MAPP composite has much lower THR than that of PP and PP/APP composites. The reason is mainly due to the fact that "polyurethane-like" microcapsules can increase the flame retardant properties of MAPP in PP matrix by way of gas and condensed flame retardant process. Except that, the residual weight of neat PP is little, which illustrates pure PP cannot form the char layer during combustion. This is the main reason for the flammability of PP materials. For PP/APP and PP/MAPP, the residual weight is 21.1 and 16.7 wt.%, respectively. Due to the thermal degradation of MEL on the PU shells in gas phase, the residual weight of PP/MAPP after cone calorimeter tests is lower than that of PP/APP, which can enhance the gas phase flame retardant action by the inert gases release from MEL. Besides, the esterified product formed via the chemical reaction between PPA and PER from PU microcapsules can greatly enhance the quality of char layer in condensed phase during combustion, which may be the main reason for the improving of flame retardant properties for PP composites. Based on these facts, compared with PP/APP, the flame retardancy of PP composites is improved by combining MAPP, which is well consistent with the results of LOI and UL-94 tests.

Table 4 Data of cone calorimeter for PP composites

Sample code	Time to ignition (s)	PHRR (kW/m^2)	THR (MJ/m^2)	Residual weight (wt%)
PP	40	1174.7	102.2	0
PP/APP	38	526.5	80.6	21.1
PP/MAPP	30	301.8	65.1	16.7

Fig. 10 Thermal degradation curves of PP composites, **a** TGA curves of PP composites, **b** DTG curves of PP composites
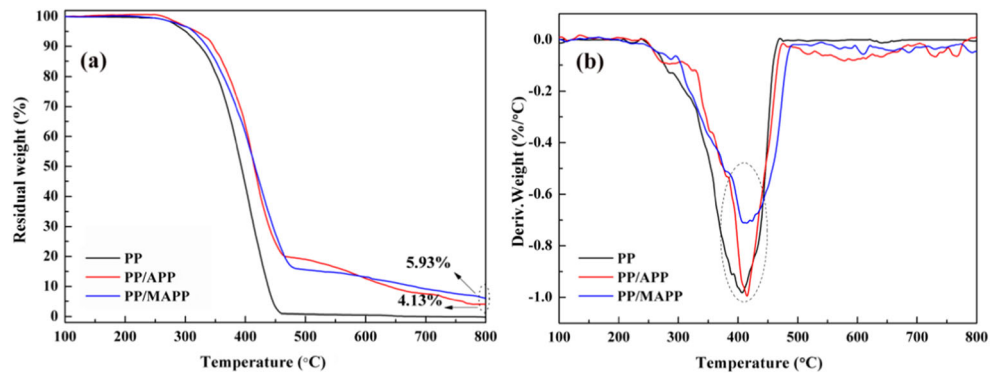
Thermal analysis of PP composites

The thermal degradation of PP, PP/APP and PP/MAPP was investigated by TGA, as shown in Fig. 10. Besides, the differential thermal gravity (DTG) of experimental and calculated TGA curves was also investigated, as shown in Fig. 10b. The detailed data is listed in Table 5, which includes the temperature at 5 % weight loss (T_{on}), the maximum weight-loss temperature (T_{max}) and the residual weight at 500, 600 and 700 °C, respectively. As shown in Fig. 10a, the initial degradation temperature of PP/MAPP is lower than that of PP/APP, which is ascribed to the thermal stability of PU shell on the surface of MAPP is lower than APP. However, the T_{max} value of PP/MAPP is slightly higher than PP/APP, as shown in Fig. 10b. Except that, the maximum decomposition rate (R_{max}) of PP/MAPP is much lower than that of PP/APP. These facts indicate that the thermal stability of PP/MAPP during thermal degradation is enhanced and the decomposition rate of PP composites slows down by compositing with MAPP, which is in agreement with the thermal decomposition of APP and MAPP in Fig. 4. The detailed reason and reaction process of PP composites is systematically depicted as follows. Moreover, it is observed that the residual weight of PP/APP at 500 °C is much higher than that of PP/MAPP. With the temperature on, the char residue weight of PP/APP decreases much faster than PP/MAPP [39]. Besides, residual weight of

PP/MAPP (13.44 %) has exceeded PP/APP (12.54 %) at 600 °C. Thus, it can be observed that the PU microcapsules on the surface of MAPP can promote the chemical reaction with APP to slow down the thermal decomposition of PP composites. Furthermore, compared with PP/APP, these facts can illustrate the increased flame retardant properties of PP/MAPP via the formation of crosslinking structure between PU microcapsules and APP in the char residue. Therefore, it can illustrate and certify the results of LOI, UL-94 and cone calorimeter tests.

The analysis of char residue for PP/MAPP after combustion

The char residue of PP/APP and PP/MAPP after combustion was studied by optical photos. As shown in Fig. 11. Compared with the inconsecutive char residue for PPAPP, the char residue structure of PP/MAPP is much compact and dense, which can restrain both mass and heat transfer between gas phase and condensed phase and protect the underlying material from further decomposition. Thus, the flame retardant properties of PP composites are improved by the formation of compact char layer. Based on these facts, the flame retardancy of PP is enhanced by compositing with MAPP. These results are in accordance with the results of LOI and cone calorimeter tests.

Furthermore, the chemical structure of residue of PP/MAPP after combustion was investigated by FTIR spectra, as shown in Fig. 12. It can be found that the absorption around 3,400 cm^{-1} is ascribed to N-H groups. The stretching vibration peak around 1,640 cm^{-1} is due to P-OH characteristic absorption. Moreover, the peak at 1,200 cm^{-1} is ascribed to P = O groups. Additionally, the peaks at 1,130 cm^{-1} represent the C-O-C groups, which may be originated by the reaction among PU microcapsules during thermal degradation. Except that, the peak at 925 cm^{-1} comes from the characteristic absorption of P-O-P groups (from P_2O_5 or P_4O_{10}) that may be originated from the decomposition products of the excess acid source (APP). Most of all, 1,008 and 794 cm^{-1} are for the symmetric stretching of P-O bond in P-O-C structure [40, 41]. Thus, the thermal decomposition process can be concluded as

Table 5 TGA data of PP composites

Sample code	T_{on}[a] (°C)	T_{max}[b] (°C)	Char residues (%)			R_{max}[c] (%/°C)
			500 °C	600 °C	700 °C	
PP	300.1	406.8	0	0	0	−0.986
PP/APP	318.6	414.4	19.13	12.54	7.55	−0.998
PP/MAPP	313.5	423.2	15.50	13.44	9.35	−0.714

[a] T_{on}: the temperature at 5 % weight loss
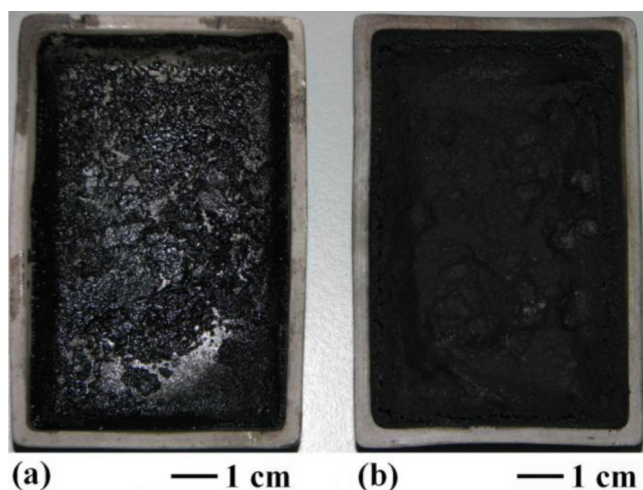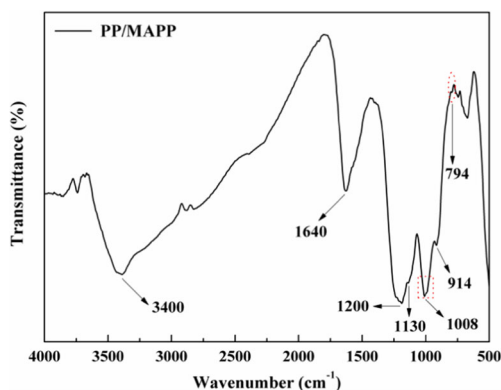
[b] T_{max}: the temperature at maximum weight-loss rate
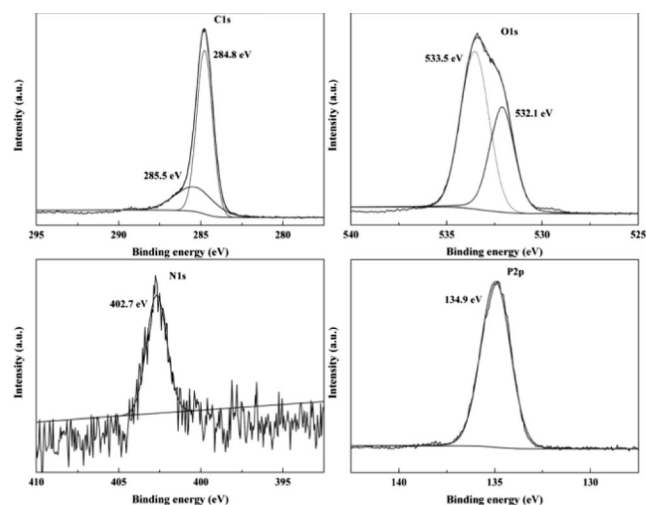
[c] R_{max}: maximum decomposition rate

Fig. 11 The optical photos of char residue of PP composites after combustion, **a** PP/APP, **b** PP/MAPP

Fig. 13 XPS spectra of char residue of PP/MAPP composites after the combustion

follows. First, APP decomposes to release NH_3 and H_2O in gas phase and form PPA (P-O-P groups) in condensed phase. In the same time, PPA from the initial degradation of APP may react with PER on PU shells to produce the "ester-like" materials, which leads to the formation of P-O-C cross-linking groups with high thermal stability. By this way, the compact and dense char layer for MAPP in PP composites is formed. And the quality of char layer (thermal stability and compactness) is improved during combustion of PP/MAPP, which can effectively slow down the thermal decomposition rate of PP composites. Thus, compared with PP/APP, the flame retardant properties of PP matrix by combining with MAPP are enhanced via the interaction and crosslinking reaction between APP and PU microcapsules.

As we know, x-ray photoelectron spectroscopy (XPS) can provide further information about elemental composition and the elemental content of char residue in detail, which supplements the results from FTIR spectra. The XPS spectra of C_{1s}, O_{1s}, N_{1s} and P_{2p} of the char residue from PP/MAPP composites after the combustion tests are shown in Fig. 13. Besides, the detailed assignations of these peaks are systematically

recorded in Table 6. Two bands of C_{1s} spectra are observed with the binding energy at 284.8 and 285.5 eV, respectively. They can be assigned to the C-H and C-C bonds in aliphatic and aromatic structures and the C-O bond in the P-O-C groups in ether and phosphate, which is well consistent with the results of FTIR spectra above. Moreover, the XPS spectra of O_{1s} presents two bands with the binding energy at 532.1 and 533.5 eV. The bands at 532.1 and 533.5 eV could be assigned to the -O- group and = O- group, respectively [7, 42, 43]. The band at 532.1 eV is mainly contributed by the P-O in the P-O-C groups, while the peak at 533.5 eV is ascribed to the P = O group. In addition, the XPS spectra of N_{1s} exhibits a peak with binding energy at 402.7 eV, which can be assigned to the nitrogen in the quaternary nitrogen in NH_4^+, respectively [44–47]. But the content of N element in the char residue is only 2 %, which is mainly converted into inert gases (NH_3) during thermal decomposition. These inert gases can take effect in gas phase that dilute the concentration of oxygen around the fire during the combustion of PP composites. As for the XPS spectra of P_{2p}, a band is found with binding energy at 134.9 eV, which can be assigned to the P-O-C groups [47–50], which can further verify the esterification reaction between APP and PU microcapsules during thermal

Fig. 12 FTIR spectra of char residue of PP/MAPP after combustion

Table 6 Element identification of functional groups of char residue from PP/MAPP composites after combustion

Element	Element content (%)	Binding energy (eV)	Group
C_{1s}	59.56	284.8	C-H or C-C
		285.5	C-O and P-O-C
O_{1s}	26.33	532.1	-O- group
		533.5	P = O group
N_{1s}	2	402.7	NH_4^+
P_{2p}	12.11	134.9	P-O-C

decomposition of PP composites. And this chemical structure can promote the thermal stability and integrity of char residue for PP composites that is known as condensed flame retardant mechanism.

Potential flame-retardant mechanism

As abovementioned results, it is obviously concluded that when MAPP was incorporated into PP matrix, the flame retardant properties of PP composites are improved. Even though the detailed flame-retardant mechanism is still not very clear, the results have also considerable and promising potential applications. In our work, based on the obtained results, the possible flame retardant mechanism is speculated as follows. First, APP and PU microcapsules start to decompose and produce the inert gases (NH_3 and H_2O). On one hand, they can dilute the oxygen concentration around the fire, which can slow down the thermal decomposition process of PP matrix; on the other hand, these gases can carry off the heat releasing from the combustion zone of PP composites. Both of two ways can accomplish the gas phase flame retardant action of MAPP in PP composites. After that, the thermal degradation products from APP and microcapsules can react and hydrate with each other to form the P-O-C groups (Figs. 11

and 13), which can promote the formation of dense and integrated char layer on the surface of PP composites during combustion. Here, APP and microcapsules play a part in the acid source and char agent in the flame-retarding system, respectively. Furthermore, this char residue can greatly limit the mass and heat transfer between gas phase and condensed phase and protect the underlying substrate from further thermal decomposition. This can be demonstrated by the digital photographs of the char residue after combustion (Fig. 12). Therefore, the flame retardant system undergoes the classic condensed flame retardant mechanism. Based on these facts, it can be summarized that the improved flame retardant properties of PP composites are ascribed to the combination of gas and condensed flame retardant mechanism. Consequently, the possible flame retardant mechanism is depicted in Scheme 3.

Conclusions

In this paper, APP particles were microencapsulated via a two-step surface polymerization method, which introduces the carbon source and blowing agent into the microcapsules simultaneously. The chemical composition of MAPP is certified by FTIR spectra. SEM photos show that the dispersion of

Scheme 3 The possible flame retardant mechanism of MAPP in PP composites
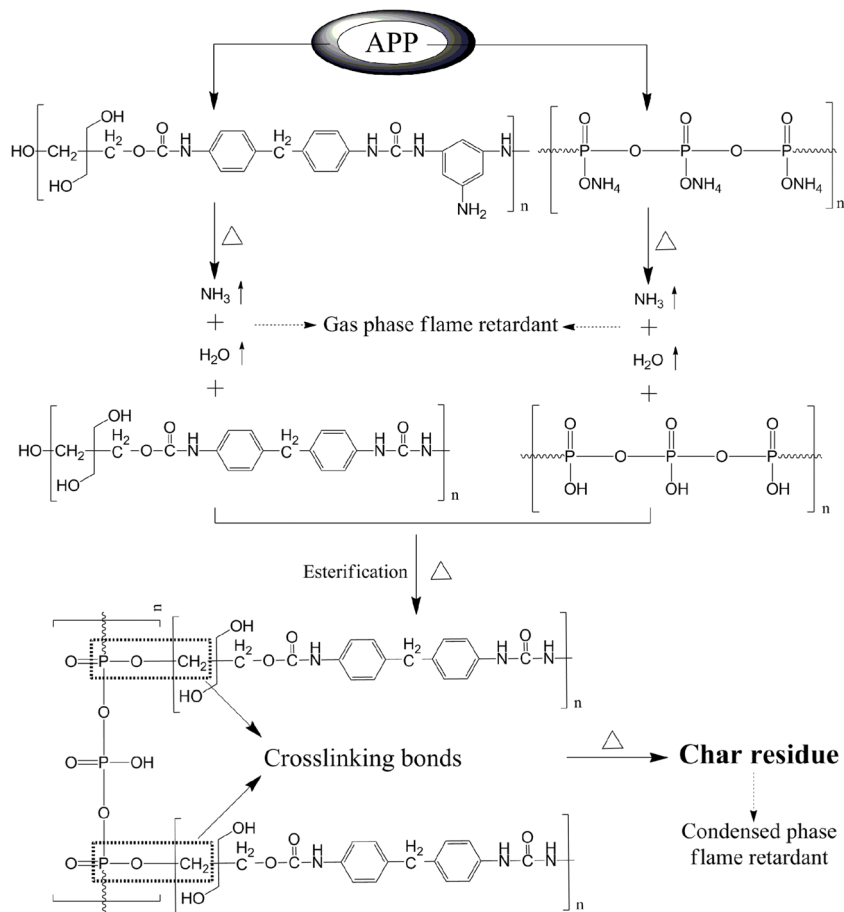
MAPP becomes better and the surface morphology of MAPP has obvious change after microencapsulation. Compared with pure APP, the water solubility of MAPP particles greatly decreases at different temperature. Besides, the water contact angle of MAPP is much larger than that of APP, which demonstrates the hydrophobic property of MAPP is enhanced after microencapsulation. It is feasible to promote the dispersion of MAPP in PP matrix. LOI and UL-94 tests of PP composites indicate the flame retardant properties of PP/MAPP are improved than that of PP/APP. The thermal degradation of PP composites by TGA and DTG illustrate the thermal behavior of PP/MAPP is different with PP/APP which is due to the thermal decomposition of PU microcapsules and the formation of crosslinking bonds between APP and PER (from microcapsules). Furthermore, the flame retardant properties of PP composites were investigated by cone calorimeter tests. The results reveal that the p-HRR value of PP/MAPP is greatly reduced, which is well consistent with the results of LOI and UL-94 tests. The char residue after combustion was analyzed by FTIR and XPS spectra. As shown in photos, an integrated and compact char layer is obtained for PP/MAPP in contrast with PP/APP. The FTIR and XPS spectra of residue interprets the formation mechanism of char layer of MAPP and the effect of PU shell on the flame retardant properties of PP/MAPP matrix. Except that, a possible flame retardant mechanism of MAPP in PP matrix is proposed.

References

1. Lv P, Wang ZZ, Hu Y et al (2009) Study on effect of polydimethylsiloxane in intumescent flame retardant polypropylene. J Polym Res 16(2):81–89
2. Chen XL, Jiao CM (2009) Synergistic effects of hydroxy silicone oil on intumescent flame retardant polypropylene system. J Polym Res 16(5):537–543
3. Wu Q, Qu BJ (2013) Synergistic effects of silicotungstic acid on intumescent flame-retardant polypropylene. Polym Degrad Stab 74(2):255–261
4. Chen XC, Ding YP, Tang T (2005) Synergistic effect of nickel formate on the thermal and flame-retardant properties of polypropylene. Polym Int 54(6):904–908
5. Chen YJ, Guo ZH, Fang ZP (2012) Relationship between the distribution of organo-montmorillonite and the flammability of flame retardant polypropylene. Polym Eng Sci 52(2):390–398
6. Gao SL, Li B, Bai P, Zhang SQ (2011) Effect of polysiloxane and silane-modified SiO2 on a novel intumescent flame retardant polypropylene system. Polym Adv Technol 22(12):2609–2616
7. Liu Y, Zhao J, Deng CL, Chen L et al (2011) Flame-retardant effect of sepiolite on an intumescent flame-retardant polypropylene system. Ind Eng Chem Res 50(4):2047–2054
8. Zuo JD, Su YK, Liu SM, Sheng Q (2011) Preparation and properties of FR-PP with phosphorus-containing intumescent flame retardant. J Polym Res 18(5):1125–1129
9. Bourbigot S, Le Bras M, Duquesne S et al (2004) Recent advances for intumescent polymers. Macromol Mater Eng 289(6):499–511
10. Le Bras M, Bourbigot S, Delporte C et al (1996) New intumescent formulations of fire-retardant polypropylene-discussion of the free radical mechanism of the formation of carbonaceous protective material during the thermo-oxidative treatment of the additives. Fire Mater 20(4):191–203
11. Almeras X, Le Bras M, Hornsby P et al (2003) Effect of fillers on the fire retardancy of intumescent polypropylene compounds. Polym Degrad Stab 82(2):325–331
12. Almeras X, Le Bras M, Poutch F et al (2003) Effect of fillers on fire retardancy of intumescent polypropylene blends. Macromol Symp 198(1):435–448
13. Le Bras M, Bugajny M, Lefebvre JM et al (2000) Use of polyurethanes as char-forming agents in polypropylene intumescent formulations. Polym Int 49(10):1115–1124
14. Zhang YJ, Lu YB, Guo F et al (2012) Preparation of microencapsulated ammonium polyphosphate with montmorillonite-melamine formaldehyde resin and its flame retardancy in EVM. Polym Adv Technol 23(2):166–170
15. Wu K, Wang ZZ, Liang HJ et al (2008) Microencapsulation of ammonium polyphosphate: preparation, characterization, and its flame retardance in polypropylene. Polym Compos 29(8):854–860
16. Wu K, Shen MM, Hu Y (2011) Synthesis of a novel intumescent flame retardant and its flame retardancy in polypropylene. J Polym Res 18(3):425–433
17. Wu K, Wang ZZ, Hu Y (2008) Microencapsulated ammonium polyphosphate with urea-melamine-formaldehyde shell: preparation, characterization, and its flame retardance in polypropylene. Polym Adv Technol 19(8):1118–1125
18. Liu L, Zhang YN, Li L et al (2011) Microencapsulated ammonium polyphosphate with epoxy resin shell: preparation, characterization, and application in EP system. Polym Adv Technol 22(12):2403–2408
19. Wu K, Song L, Wang ZZ et al (2008) Microencapsulation of ammonium polyphosphate with PVA-melamine-formaldehyde resin and its flame retardance in polypropylene. Polym Adv Technol 19(12):1914–1921
20. Sun CY, Zhang QB, Li B (2007) The water resistance of surface-modified APP with melamine-TD I in LLDPE. J Polym Res 14(6):505–509
21. Zheng ZH, Yan JT, Sun HM et al (2013) Preparation and characterization of microencapsulated ammonium polyphosphate and its synergistic flame-retarded polyurethane rigid foams with expandable graphite. Polym Int. doi:10.1002/pi.4477
22. Lan YH, Li DH, Yang RJ et al (2013) Computer simulation study on the compatibility of cyclotriphosphazene containing aminopropylsilicone functional group in flame retarded polypropylene/ammonium polyphosphate composites. Compos Sci Technol 88(14):9–15
23. Ni JX, Tai QL, Lu HD et al (2010) Microencapsulated ammonium polyphosphate with polyurethane shell: preparation, characterization, and its flame retardance in polyurethane. Polym Adv Technol 21(6):392–400
24. Chen DK, Li J, Ren J (2011) Combustion properties and transference behavior of ultrafine microencapsulated ammonium polyphosphate in ramie fabric-reinforced poly(L-lactic acid) biocomposites. Polym Int 60(4):599–606
25. Wu Q, Lü JP, Qu BJ (2011) Preparation and characterization of microcapsulated red phosphorus and its flame-retardant mechanism in halogen-free flame retardant polyolefins. Polym Int 52(8):1326–1331
26. Sun LH, Qu YT, Li SX (2012) Co-microencapsulate of ammonium polyphosphate and pentaerythritol and kinetics of its thermal degradation. Polym Degrad Stab 97(3):404–409
27. Zheng ZH, Sun HM, Li WJ et al (2013) Co-microencapsulation of ammonium polyphosphate and aluminum hydroxide in halogen-free

and intumescent flame retarding polypropylene. Polym Compos. doi: 10.1002/pc.22715

28. Zheng ZH, Li WJ, Sun HM et al (2013) Preparation and characterization of polystyrene/modified carbon black composite beads via in situ suspension polymerization. Polym Compos 34(7):1110–1118

29. Ni JX, Chen LJ, Zhao KM et al (2011) Preparation of gel-silica/ ammonium polyphosphate core-shell flame retardant and properties of polyurethane composites. Polym Adv Technol 22(12):1824–1831

30. Wu K, Song L, Wang ZZ et al (2009) Preparation and characterization of double shell microencapsulated ammonium polyphosphate and its flame retardance in polypropylene. J Polym Res 16(3):283–294

31. Chen XL, Jiao CM, Zhang J (2011) Microencapsulation of ammonium polyphosphate with hydroxyl silicone oil and its flame retardance in thermoplastic polyurethane. J Therm Anal Calorim 104(3):1037–1043

32. Lei ZQ, Cao YM, Xie F (2012) Study on surface modification and flame retardants properties of ammonium polyphosphate for polypropylene. J Appl Polym Sci 124(1):781–788

33. Ni JX, Song L, Hu Y et al (2009) Preparation and characterization of microencapsulated ammonium polyphosphate with polyurethane shell by in situ polymerization and its flame retardance in polyurethane. Polym Adv Technol 20(12):999–1005

34. Akten ED, Mattice WL (2001) Monte Carlo simulation of head-to-head, tail-to-tail polypropylene and its mixing with polyethylene in the melt. Macromolecules 34(10):3389–3395

35. Liao RJ, Zhu MZ, Zhou X (2012) Molecular dynamics study of the disruption of H-bonds by water molecules and its diffusion behavior in amorphous cellulose. Mod Phys Lett B 26(14):1250088-14

36. Zhu XS, Pan QQ, Xu HS et al (2010) Effects of coal and ammonium polyphosphate on thermal degradation and flame retardancy of polyethylene terephthalate. J Polym Res 17(5):621–629

37. Zhang Q, Chen YH (2011) Synergistic effects of ammonium polyphosphate/melamine intumescent system with macromolecular char former in flame-retarding polyoxymethylene. J Polym Res 18(2):293–303

38. Hsiue GH, Wang WJ, Chang FC (1999) Synthesis, characterization, thermal and flame-retardant properties of silicon-based epoxy resins. J Appl Polym Sci 73(7):1231–1238

39. Song PA, Fang ZP, Tong LF (2009) Synthesis of a novel oligomeric intumescent flame retardant and its application in polypropylene. Polym Eng Sci 49(7):1326–1331

40. Li J, Ke CH, Xu L et al (2012) Synergistic effect between a hyperbranched charring agent and ammonium polyphosphate on the intumescent flame retardance of acrylonitrile-butadiene-styrene polymer. Polym Degrad Stab 97(7):1107–1113

41. Mahapatra SS, Karak N (2007) s-Triazine containing flame retardant hyperbranched polyamines: synthesis, characterization and properties evaluation. Polym Degrad Stab 92(6):947–955

42. Zhao CX, Liu Y, Wang DY, Wang DL et al (2008) Synergistic effect of ammonium polyphosphate and layered double hydroxide on flame retardant properties of poly(vinyl alcohol). Polym Degrad Stab 93(7):1323–1331

43. Dittrich B, Wartig KA, Hofmann D et al (2013) Flame retardancy through carbon nanomaterials: carbon black, multiwall nanotubes, expanded graphite, multi-layer graphene and graphene in polypropylene. Polym Degrad Stab 98(8):1495–1505

44. Huang GB, Liang HD, Wang Y et al (2012) Combination effect of melamine polyphosphate and graphene on flame retardant properties of poly(vinyl alcohol). Mater Chem Phys 132(2–3):520–528

45. Wang X, Li Y, Liao W et al (2008) A new intumescent flame-retardant: preparation, surface modification, and its application in polypropylene. Polym Adv Technol 19(8):1055–1061

46. Hu X, Guo Y, Chen L et al (2012) A novel polymeric intumescent flame retardant: synthesis, thermal degradation mechanism and application in ABS copolymer. Polym Degrad Stab 97(9):1772–1778

47. Liu W, Chen DQ, Wang YZ et al (2007) Char-forming mechanism of a novel polymeric flame retardant with char agent. Polym Degrad Stab 92(6):1046–1052

48. Wang ZY, Han EH, Ke W (2005) Influence of nano-LDHs on char formation and fire-resistant properties of flame-retardant coating. Prog Org Coat 53(1):29–37

49. Ke CH, Li J, Fang KY et al (2010) Synergistic effect between a novel hyperbranched charring agent and ammonium polyphosphate on the flame retardant and anti-dripping properties of polylactide. Polym Degrad Stab 95(5):763–770

50. Qu BJ, Xie RC (2003) Intumescent char structures and flame-retardant mechanism of expandable graphite-based halogen-free flame-retardant linear low density polyethylene blends. Polym Int 52(9):1415–1422